Ying and Xi *Int J Concr Struct Mater* (2022) 16:8
https://doi.org/10.1186/s40069-021-00494-5

International Journal of Concrete Structures and Materials

RESEARCH Open Access

Microstructure and Chloride Diffusion Properties of Hardened Fly Ash Cement Paste with Three-dimensional Graphene

Jingwei Ying[1,2*] and Xiaoying Xi[1]

Abstract

In this paper, the influence of three-dimensional graphene (3DG) on the microstructure and chloride diffusion properties of fly ash cement paste was investigated. 3DG accounting for 0.0–0.2% of cement mass was evenly dispersed in hardened cement paste containing fly ash by using ultrasonic and polycarboxylate superplasticizer. The microstructure of the cement paste was characterized by mercury intrusion test (MIP), X-ray diffraction (XRD), and scanning electron microscope (SEM). The results indicate that an appropriate amount of 3DG accelerates the secondary hydration of fly ash and provides a platform for the growth of cement hydration crystals. Moreover, the hydrated crystal fills the pores, reduces the harmful porosity, and refines the pore structure. The enhanced microstructure significantly improved mechanical properties and chloride diffusion resistance of hardened fly ash cement. With the addition of 0.1% 3DG, the compressive strength increased by 31.33%, and the chloride diffusion coefficient was reduced by 49.44%. The findings are beneficial to promote the generalized application of 3DG in cement in the marine environment.

Keywords: three-dimensional graphene, fly ash, mechanical properties, chloride diffusion, microstructure

1 Introduction

As an important building material in ocean structural engineering, the corrosion of sulfate and chloride ions seriously endangers the safety and durability of concrete structures (Ariyachandra et al., 2021; Li et al., 2020; Park & Choi, 2012). Concrete is a porous material with many pores and cracks inside. The cracks in the concrete structure (Morga & Marano, 2015; Nguyen et al., 2017) and the chloride concentration gradient in the seawater lead to chloride diffusion in the concrete (Jiang et al., 2019). It is easy to induce damage and affect the average service life of the structure. However, studies have shown that the use of supplementary cement materials (SCMs) can significantly impact the transport of chloride in concrete.

Fly ash (FA), as industrial waste, has been widely used as a partial substitute for cement (Park & Choi, 2012; Yu et al., 2017; Zhao et al., 2020a). The utilization of fly ash as partial replacement to cement reduces production costs and enhances the property of hardened cementitious composites. The workability of cement-based materials improved because of the morphological effect of fly ash (Zhang et al., 2019a). In addition, fly ash has contributed to the improvement of the pore structure and microstructure of cement in active effect and micro-aggregate effect (Shen & Zhang, 1981), which further provide enhanced mechanical strength (Hefni et al., 2018) and durability (Yamato et al., 2020). However, the early strength of cement-based materials develops slowly due to the addition of fly ash (Du et al., 2020; Kaur et al., 2020; Wu et al., 2018).

*Correspondence: yingjingwei@gxu.edu.cn
[1] School of Civil Engineering and Architecture, Guangxi University, Nanning 530004, China
Full list of author information is available at the end of the article
Journal information: ISSN 1976-0485 / eISSN 2234-1315

The emergence of nanomaterials provides a new direction for improving the early mechanical properties. Nanomaterials, such as nano-SiO_2, nano-Fe_2O_3, and carbon nanotubes, have been proven to effectively enhance the performance of cement-based materials (Konstantopoulos et al., 2020; Mittal et al., 2015; Zhang et al., 2019b). Graphene nanomaterials have attracted the attention of researchers because of their high strength and large specific surface area (Muthu et al., 2021). The compressive strength, tensile strength, and flexural strength of cement composites improved with GO up to 0.03%. The addition of GO regulated the hydration products to form dense flower-like and polyhedral-like shapes (Lv et al., 2013, 2014a; 2014b). In addition, graphene derivatives, such as GO (Zhao et al., 2020b) and graphene nanoplates (GNP) (Du & Dai, 2015; Du et al., 2016), reduced the average diffusion depth of chloride and chloride diffusion coefficient. The improved barrier properties were attributed to the enhanced pore structure and the dense microstructure induced by graphene. At the same time, it was found that GO-modified cement can form a three-dimensional network structure, and the formation mechanism was also illustrated (Li et al., 2018; Wang et al., 2016). Therefore, in addition to the nanofilling effect, graphene can significantly improve the macroscopic performance of cement-based materials by influencing the morphology of hydration products, template effect, and bridging mechanism.

Based on the strengthening effect of graphene in cement, graphene also has been used in fly ash cement composite to improve its properties. The mechanical property of hardened fly ash cement paste increased when adding 0.125% GO, which was synthesized from mechanically milled graphite (Sharma et al., 2018). The microstructure of hardened fly ash cement composite was refined by controlling the orientation of the hydration crystal. As reported in prior studies (Wang et al., 2017, 2019a), the combination of 0.01% GO and 20% fly ash had the best performance. The addition of fly ash could improve the fluidity of the GO cement system. The acceleration of the pozzolanic effect of fly ash, the reduction of harmful pores volume, and the refinement of calcium hydroxide crystal were helpful to improve the mechanical strength of the GO-FA-cement composite. In addition, mixed functionalized carbon nanotubes (FCNTs) and GO had a better ability over individual GO or FCNTs in the FA-cement mortars (Kaur & Kothiyal, 2020). Previous studies have shown that two-dimensional graphene shows a good reinforcement effect in fly ash cement-based materials. However, the re-stacking caused by the poor dispersion ability of graphene severely inhibits its enhancement effect.

To maintain its unique characteristics and expand the practical application of graphene, researchers try to construct a three-dimensional graphene structure. At present, three-dimensional graphene has been widely studied in batteries (Li et al., 2019) and supercapacitors (Luo et al., 2019) because of its low density and unique three-dimensional connection electronic transmission network. Moreover, three-dimensional graphene is ideal for seawater desalination (Wang et al., 2019b) and environmental pollutant management (Lai et al., 2019). The large surface area and its well-defined porous structure enhance the opportunity to contact pollutants, which is conducive to the diffusion of pollutant molecules into the three-dimensional structure. Therefore, the above advantages of three-dimensional graphene are of positive significance to improving the properties of cement-based composites.

Based on the above advantages, 3DG, a new graphene material, was used in the fly ash cement paste for the first time in this study. The effect of 3DG on micromorphology, fluidity, mechanical strength, and durability of fly ash cement paste was systematically investigated in this paper. Firstly, 3DG was dispersed by combining ultrasonic crusher and dispersant, and the cement paste was prepared. Then the fluidity was measured using a mini-slump cone. The compressive strength and chloride ion diffusivity of hardened fly ash cement samples were also tested. In addition, techniques, including mercury intrusion porosimeter (MIP), X-ray diffraction (XRD), and scanning electron microscopy (SEM), were employed to characterize the influence of 3DG on the microstructure of fly ash cement paste.

2 Experimental

2.1 Materials

The cement used in this research was PO 42.5 ordinary Portland cement complying with the China National Standard GB175-2007. It was obtained from Fusui Xinning Conch Cement Co., Ltd. Class I fly ash was procured from Gongyi Yuanheng water purification material factory (Gongyi, Henan). In addition, fly ash was used at a dosage of 20% as a partial replacement to ordinary portland cement (OPC) in the mixes. The chemical composition of cement and fly ash is presented in Table 1. The 3DG used in this research was developed by the team of Shen from the Graphene Research Center of Guangxi University (Shen et al., 2016). Graphene is economical and applicable, with a wide range of raw materials. The physical properties are shown in Table 2. The SEM images of three-dimensional graphene are shown in Fig. 1. Graphene is gathered and stacked together in a three-dimensional honeycomb structure in the figure. A

Table 1 Chemical composition of cement and fly ash (wt.%).

	SiO_2	Al_2O_3	Fe_2O_3	CaO	SO_3	MgO	P_2O_5
Cement	22.09	6.7	4.43	58.13	2.22	0.87	–
Fly ash	58.6	15.3	14.4	4.11	0.92	1.26	1.87

Table 2 Properties of three-dimensional graphene.

Properties	Description
Specific surface area	$\geq 600\ m^2/g$
Pore size distribution	10^{-9}–10^{-5} m
Porosity	≥ 30.0%
Fineness	$\geq 10^{-7}$ m
Electrical conductivity	1000 s/m (25 Mpa)
Impurity metal content	≤ 2%

highly efficient polycarboxylate superplasticizer (PC) was used as a dispersant.

2.2 Preparation of Graphene Dispersion

For 3DG to manifest its superior properties, 3DG must be well dispersed in the cement matrix. The 3DG has a small particle size and a large specific surface area. There is a large van der Waals force between the nanoparticles, and untreated nanoparticles are prone to aggregate. Furthermore, these aggregations may appear later as defects in the paste and reduce the mechanical performance of the composites. Thus, it is necessary to improve the graphene dispersity before mixing cement materials.

Ultrasonic dispersion or mechanical stirring alone cannot achieve a good dispersion effect. Chemical treatments of 3DG through copolymer modification are complex, making it unsuitable for industrial applications. In order to make 3DG uniformly and stably combined with cement-based composites, the functions of ultrasonic dispersion and surfactants were experimentally utilized to disperse graphene in aqueous solution referring to the method of researchers from Du and Pang (2018), Tragazikis et al. (2019), and Liu et al. (2019). In this experiment, a type ultrasonic instrument of the HSD-1800Y model (50 kHz, 1800 W) was used to disperse 3DG, which was supplied by Ningbo high tech Zone Oulan Technology Co., Ltd. (Ningbo, China). The sample preparation steps were carried out as follows:

(1) Firstly, the required 3DG, polycarboxylate superplasticizer, and water were weighed.
(2) Then, 3DG was placed in water and stirred until the graphene was thoroughly wetted. After that, a polycarboxylate superplasticizer was added slowly to this solution according to the mass ratio of 3DG:PC = 1:1.
(3) An ultrasonic disrupter was used to reduce the aggregation of 3DG in water. And the total sonication time was controlled at 20 min. The suspension was placed in ice water to prevent foaming and heating caused by the sonication process.
(4) Take out the dispersion after 20 min.

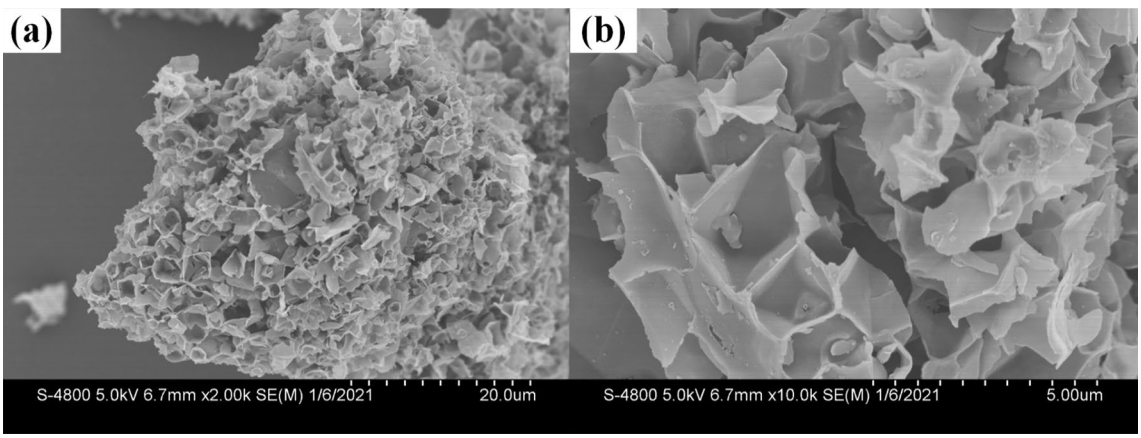

Fig. 1 SEM images of three-dimensional graphene: **a** 20 μm; **b** 5 μm.

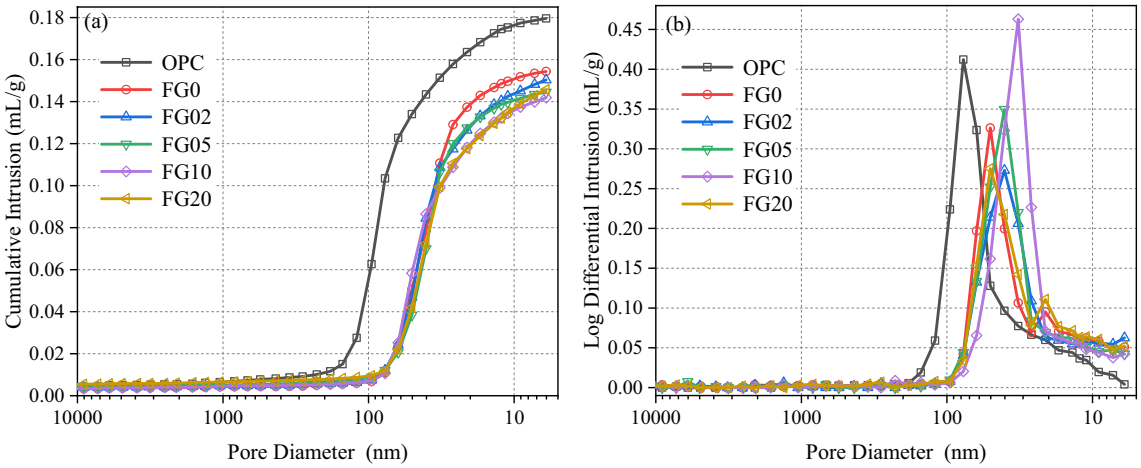

Fig. 2 Pore structure of 3DG-fly ash cement paste: **a** Cumulative intrusion curves; **b** Differential distribution curves.

Table 3 The number and composition of fly ash cement paste.

Sample	Cement/%	Fly ash/%	3DG/%	PC/%	Fluidity/mm
OPC	100	0	0	0	76
FG0	80	20	0	0	91
FG02	80	20	0.02	0.02	110
FG05	80	20	0.05	0.05	112
FG10	80	20	0.1	0.1	120
FG20	80	20	0.2	0.2	122

"0," "02," "05," "10," and "20," respectively, indicate that the weight percentage of 3DG is 0%, 0.02 wt%, 0.05 wt%, 0.1 wt%, and 0.2 wt% of cement and fly ash mixture.

F fly ash, *G* graphene with three-dimensional structure.

2.3 Specimen Preparation

In order to study the effect of three-dimensional graphene (3DG) on fly ash cementitious matrix, six different mix proportions are given in Table 3. The ratio of water to cement was 0.4 for all the preparations. The first mixture was the basic paste mixture containing 100% cement. The second mix was the reference mix containing 20% FA as partial replacement to cement, and 3DG was not added to it. The remaining four mixes were all 3DG-FA-cement samples at a 3DG proportion of 0.02%, 0.05%, 0.1%, and 0.2% (by weight of binder FA + OPC), which were labeled as FG02, FG05, FG10, and FG20, respectively. To evenly mix the mixture, the cement and fly ash were put into the mixing pot and stirred for the 60 s. Then the homogeneously dispersed 3DG suspension was mixed with cement and fly ash powders, and stirred at low speed for 3 min, then at high speed for 1 min. After that, the readily mixed cement paste was poured into molds and then vibrated for the 30 s to avoid possible air bubbles. All the specimens were wrapped with plastic films for 24 h to prevent water loss. After demolding, all the samples were placed in saturated calcium hydroxide solution for standard curing until the testing age. The specimens were dried before testing.

2.4 Testing and Characterization

2.4.1 Fluidity Measurements

In order to characterize the influence of 3DG content on the workability of fly ash cement paste, the fluidity of cement paste was tested according to the test method for homogeneity of concrete admixtures (GB/T 8077-2012). The mixtures were poured into a truncated cone mold immediately after mixing. The dimensions of the cone model were top diameter 36 mm, bottom diameter 60 mm, and height 60 mm. The cement paste was smoothed with a spatula. Then the mold was removed vertically. The maximum diameter of the fresh fly ash cement paste in two directions perpendicular to each other was measured. The average value of the two vertical directions was recorded as the final fluidity.

2.4.2 Compressive Strength Measurements

According to the Chinese standard GB/T 17671-2020, the compressive strength of samples was tested at 28days by the MTS810 hydraulic servo testing machine. The size of specimens for measurements was $40 \times 40 \times 40$ mm. The loading rate was set to 2.4 kN/s. Three specimens were repeated for compressive strengths. The average of three values was taken as representative compressive strength.

2.4.3 Chloride Diffusion Measurements

The Ion Selective Electrode method (ISE) was applied to evaluate the effect of 3DG on chloride diffusion of hardened fly ash cement paste in this study. The content of water-soluble chloride in fly ash cement-based composites was determined by the NJCL-B chloride ion rapid determination instrument (Beijing, China). The

size of the specimens was $10 \times 20 \times 30$ mm. The samples cured for 28 days were conducted with the chloride diffusion tests. In order to bond the epoxy resin tightly to the sample, the five surfaces of the dry test block were coated with epoxy resin. The uncoated epoxy surface was 10×20 mm in size and served as a chloride diffusion surface. After the epoxy resin was dried, the sample was immersed in a NaCl solution (5% by mass). After the immersion of 7 days, the specimens were removed and split along the direction of chloride diffusion. Then, a 0.1 mol/L silver nitrate solution was sprayed onto the surface of the split samples. The color change border was identified as the chloride diffusion depth. After that, half of the sample was used to investigate the chloride content at different depths. Layers of 4 mm depths (0–20 mm) were milled, and the powders were collected. After being dried at 60 ℃ for 6 h in an oven, the powders were put in the bottle with deionized water. The bottle was shaken 3–5 times before the test.

2.4.4 Microscopic Characterization

The porosity and pore structure of the hardened fly ash cement paste was tested by an Autopore IV9500 automatic mercury porosimeter (Micromeritics Co., USA) with a pressure ranges up to 228 MPa. The pore diameter was performed from 0.003 μm to 1000 μm. Cubes of size $10 \times 10 \times 10$ mm were used for MIP measurements. After 28 days of curing, the samples were soaked in acetone to stop the hydration process. Then, the samples were dried at 60 ℃ for 6 hours before MIP measurements.

The fly ash cement paste of 28 days was carried out by X-ray diffraction (Mini Flex 600) using Cu Kα radiation (λ = 1.54056 Å) and operating at 40 kV and 15 mA with a step size of 0.02. The qualitative analysis of cement hydrates was examined with a scanning rate of 4°/min in the 2θ range of 2–70 °. Powder samples of hardened fly ash cement paste were produced by grinding.

To better understand the microstructure evolution of 3DG-fly ash cement paste, the field emission scanning electron microscope (Carl Zeiss, Germany and Hitachi-SU8220, Japan) was used. The fracture surfaces of the composites after the compressive strength test were selected to characterize the morphology. Samples were dried under vacuum conditions for 6 hours before the test. The working voltage of the scanning electron microscope was 5.0 kV.

3 Results and Discussion

3.1 Microstructural Characterization

3.1.1 Pore Structure

The pore characteristics of the 3DG fly ash cement system of 28d were characterized by MIP. The cumulative and log differential intrusion curves are shown in Fig. 2. The detailed results of the mercury intrusion test are shown in Table 4. With the addition of 20% fly ash, the cumulative intrusion curve shifts down significantly in Fig. 2a. With the addition of 3DG, the cumulative intrusion curves shift downward and then upward. The sample with 0.1% content 3DG has the smallest cumulative intrusion volume. Compared with the FG0 group, the cumulative intrusion volume drops by 8.1%. The addition of fly ash and 3DG plays the synergetic role in reducing the pore volume of cement-based materials. The peak value of six specimens is mainly distributed between 10 and 100 nm in Fig. 2b. With the addition of 3DG, it is evident that the peaks of the differential distribution curves shift toward smaller pore sizes. The most probable pore size, which corresponds to the peak in the differential distribution curves, represents pore size with the highest probability. The specific data measured in the test are listed in Table 4. Compared with the reference group FG0, the most probable pore size is reduced by 19.96% with 0.02% 3DG. When the 3DG content is 0.1%, the reduction quantity reaches a maximum and the decrease is 35.67%. When the content of 3DG further increases, the most probable pore size begins to rise.

The incorporation of 3DG not only affects the porosity and the most probable pore size of cement paste but also affects its pore size distribution. According to the classification standard proposed by Wu (1979), the pore sizes can be divided into four categories, namely harmless pores (< 20 nm), less-harmful pores (20–50 nm), harmful pores (50–200 nm), and more-harmful pores (> 200 nm). The pore size distribution measured by MIP is shown in Fig. 3. Results indicate that the introduction of 3DG into the fly ash cement paste has a minor effect on both harmless pores (< 20 nm) and more-harmful pores (> 200 nm). The less-harmful pores (20–50 nm) and the harmful pores (50–200 nm) changed obviously. With the increase of 3DG content, less-harmful pores gradually become the dominant pores. The fraction of the less-harmful pores and the harmful pores are shown in Table 4. The fraction of less-harmful pores is calculated by dividing the porosity of less-harmful pores (20–50 nm) by the corresponding total porosity. The fraction of less-harmful pores in FG02, FG05, FG10, and FG20 samples are 56.18%, 52.85%, 61.67%, and 51.95%, respectively. Therefore, the addition of 3DG can refine the pore structure of the fly ash cement system and promote the transformation of the harmful pores (50–200 nm) to less-harmful pores (20–50 nm).

3.1.2 XRD Analysis

XRD was used to determine the qualitative interpretation of various phase compositions and evaluate hydration

reactions in the cement paste. The XRD results of ordinary cement paste (OPC), cement paste with 20% fly ash (FG0), and 0.1% 3DG-fly ash cement paste sample (FG10) at 28 days of curing are shown in Fig. 4. It shows that the XRD diffraction peaks of FG0 and FG10 samples are similar to ordinary cement paste. It indicates that no new hydration products generate by adding fly ash and 0.1% 3DG compared with ordinary cement paste. However, the peak intensity of the CH crystals in FG10 is stronger than in the FG0 sample. This shows that CH has better crystallinity. Thus, it is indicated that the addition of 3DG may promote hydration reactions in the cement matrix and create conditions for the secondary hydration of fly ash.

3.1.3 SEM Microstructural Analysis

In this research, SEM was employed to observe the microstructure of the cement composites. Ordinary cement paste (OPC), reference group FG0 (20% FA), and FG10 (20% FA-0.1% 3DG) samples at 28 days of curing were tested to study the effect of 3DG on the microstructure and hydration product morphology of fly ash cement paste. SEM images are shown in Figs. 5, 6, 7, respectiv ely.

Fig. 5a, b illustrates SEM images of the ordinary cement paste (OPC) cured at 28 days. There are still big and sparse holes randomly distributed in Fig. 5a, which decrease the density of the specimens. Fig. 5b presents a large number of needle-like hydration products randomly distributed throughout the matrix. And the cracks distribute in the slack hydration products in a straight manner. Thus, the structure of hydration products in ordinary cement paste is loose.

Fig. 6a, b depicts the morphology of 20% fly ash cement paste. Many spherical FA particles distributed in hydration products are shown in Fig. 6a. Some fine particles of hydration products have been adhered to the surface of FA, indicating the hydration of FA is just at the beginning stage in fly ash cement composites. At this stage, FA particles mainly play the role of filling and micro-aggregate

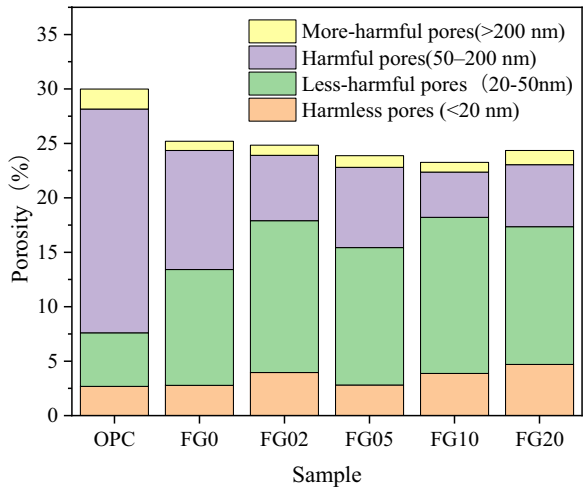

Fig. 3 Pore size distribution of 3DG-fly ash cement paste of 28 days.

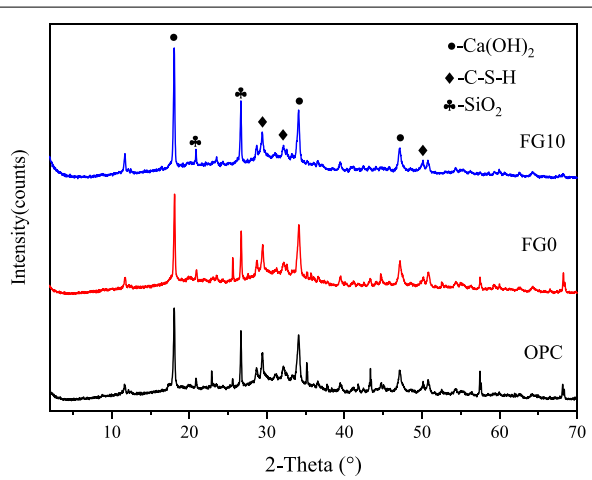

Fig. 4 XRD patterns of OPC, FG0, and FG10 at 28 days.

in cement. In addition, it is also can be observed that the continuous fine cracks pass through the cement matrix. As shown in Fig. 6b, the loose structure is C–S–H gel is

Table 4 MIP results of fly ash cement paste with different amounts of 3DG.

Sample	Porosity/%	Total intruded volume/mL/g	The most probable pore diameter/nm	Fraction of less-harmful pores/%	Fraction of harmful pores/%
OPC	30.00	0.1796	77.109	16.42	68.49
FG0	25.20	0.1543	50.35	42.22	43.36
FG02	24.84	0.1503	40.30	56.18	24.15
FG05	23.87	0.1445	40.29	52.85	30.89
FG10	23.25	0.1418	32.39	61.67	17.88
FG20	24.35	0.1457	50.38	51.95	23.39

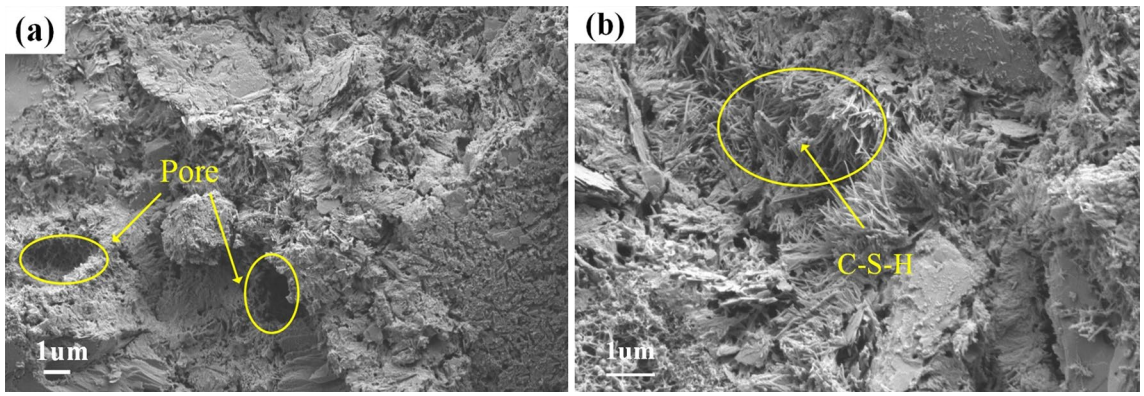

Fig. 5 SEM images of ordinary cement paste: **a** Morphology of sample surface; **b** Morphology of C–S–H.

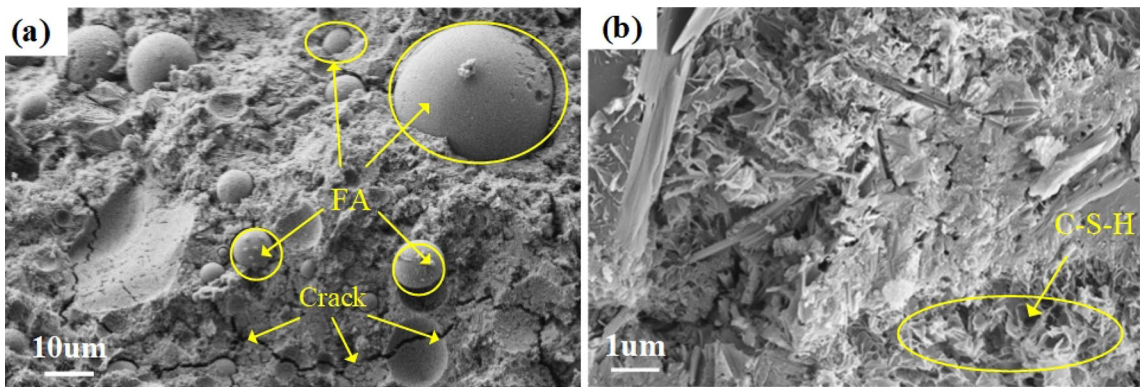

Fig. 6 SEM images of 20% fly ash cement paste: **a** Reaction degree of fly ash and **b** morphology of C–S–H.

distributed in a disorder condition. Compared with the OPC group, the morphology of C–S–H changes from fibrous to loose network structure.

Fig. 7a–i shows the microscopic morphology of the fly ash cement sample with 0.1% 3DG. It can be observed from Fig. 7a that the surface of some FA particles is uneven. Fig. 7b, c depicts the morphology of hydration products attached to the surface of fly ash particles. A small amount of CH and a large amount of particle hydration products are attached to the surface of FA particles. Compared with the FA particle in Fig. 6a, the degree of secondary hydration of FA is higher. It is indicated that the addition of 3DG has accelerated the pozzolanic reactions of FA particles. This can be attributed to the fact that three-dimensional honeycomb graphene provides nucleation sites to facilitate the precipitation of primary cement hydration products, which further triggers the secondary hydration of the FA particles (Kaur & Kothiyal, 2020). Meanwhile, the accumulated layered C–S–H can be observed around the fly ash. It shows that the combined effect of 3DG and fly ash is more beneficial to the formation of cement hydration products.

Fig. 7d–f shows the microstructure of 3DG in cement and its combination with hydration products. As shown in Fig. 7d, the three-dimensional honeycomb structure of graphene can be observed in the fly ash cement matrix. At the same time, the 3DG is closely connected with the cement matrix by providing the attachment point of hydration products. Fig. 7e, f shows the details of the connection between graphene and cement products. It can be observed that many small particles of C–S–H gel adhere to the cavity and thin wall of 3DG. 3DG is used as the nucleation site of C–S–H gel and used as a carrier to accelerate the growth of C–S–H. The continuously generated C–S–H forms a three-dimensional connecting network along the single-layer graphene wall of 3DG. The thin graphene wall acts as a bridge between the cement matrix and graphene to connect them into an integral structure. Fig. 7g shows that the dense graphene sheet is closely bonded to the cement. The dense graphene sheet can effectively block the development of cracks to prevent the diffusion of chloride ions. This can be attributed to the barrier formed by the graphene sheet, which makes the entry path of chloride ions more tortuous (Du et al., 2016). It can be observed

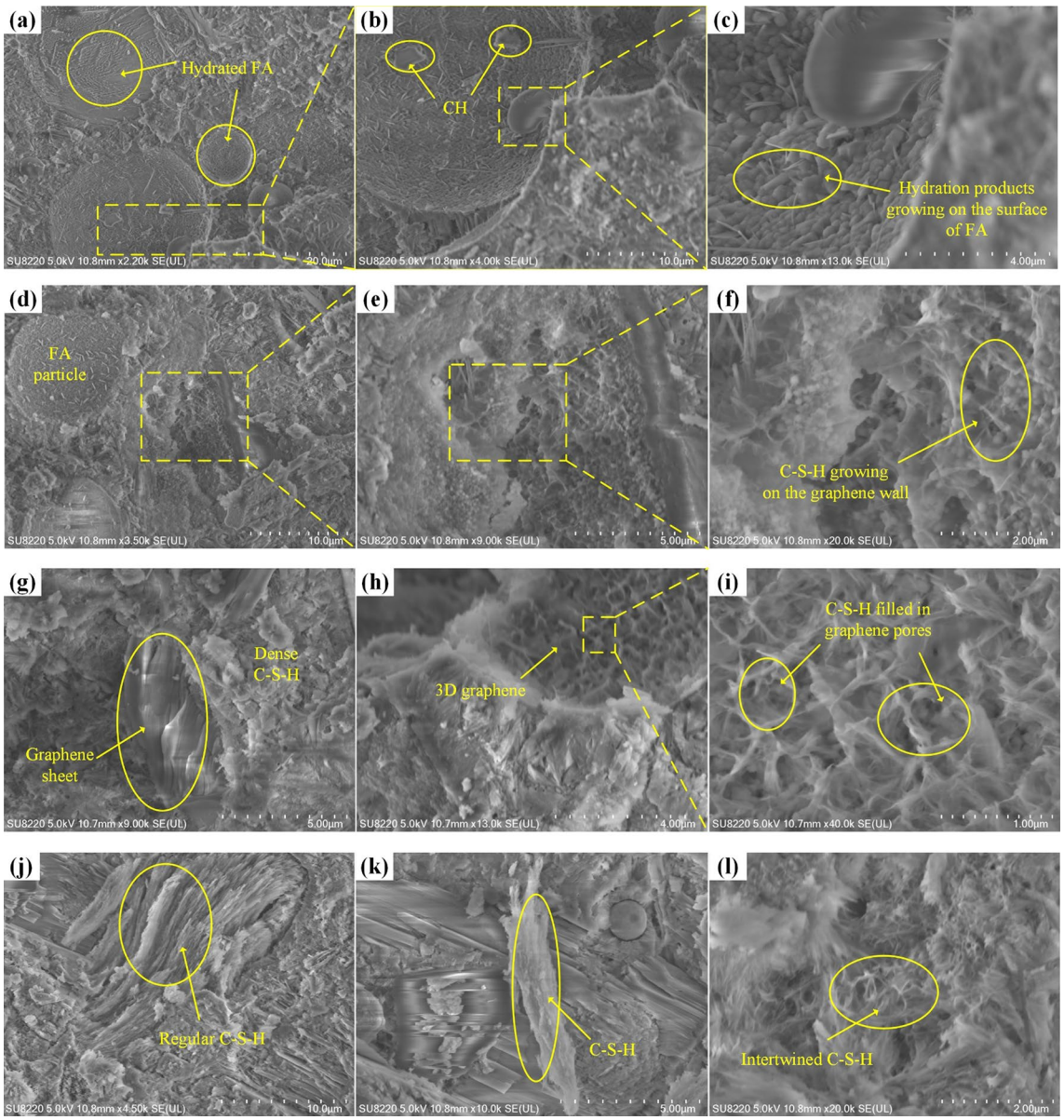

Fig. 7 SEM images of 0.1 wt% 3DG-fly ash cement paste: **a**–**c** Reaction degree of fly ash; **d**–**i** Combination of 3DG and hydration products; **j**–**l** Morphology of C–S–H.

that a stacked connecting wall is formed at the connection between graphene and cement hydration products in Fig. 7h. Fig. 7i shows the details of the three-dimensional graphene. Graphene is used as the substrate for crystal formation and deposition because of its huge specific surface area, which provides a platform for crystal formation and growth. At the same time, it can not only enhance the adhesion between cement and graphene but also prevent crack propagation to enhance the overall mechanical properties of cement-based materials (Li et al., 2018). Fig. 7j–l shows the morphology of C–S–H. Compared with C–S–H in Fig. 6b, C–S–H in Fig. 7i is denser and more regular. It is indicated that the addition of graphene and fly ash changes the trend of C–S–H and makes its arrangement more orderly. It is shown in Fig. 7l that the C–S–H are staggered, which is conducive to anchoring and bonding. The above results show that graphene can not only improve the morphology of cement hydration products but also enhance the combination of them. It helps prevent the diffusion of chloride ions and improve its mechanical properties.

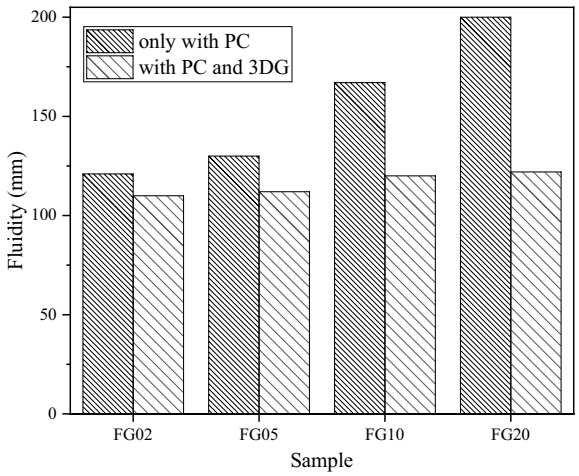

Fig. 8 The fluidity of the fly ash cement paste.

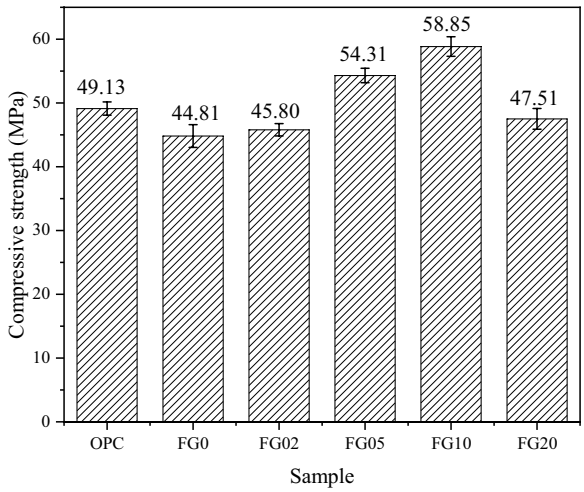

Fig. 9 Compressive strength of fly ash cement paste.

3.2 Macro Experiments Analysis

3.2.1 Flowability

In this research, a mini-slump cone test was conducted to find out the influence of 3DG on the fluidity of fly ash cement paste. At the same time, the increased content of dispersant will also affect the fluidity of cement-based materials. Therefore, fly ash cement containing different doses of dispersant was added in this experiment. And the results are given in Fig. 8. When 3DG and PC were added into fly ash cement paste at the same time, it was found that the fluidity of FG02, FG05, FG10 and FG20 groups was lower than that of fly ash cement paste containing only PC. Due to the large specific area of 3DG, flocculation shape and accumulation of cement particles are formed. The flocculated structure entraps a large amount of water which leads to lower fluidity (Indukuri et al., 2019). The fluidity diameters are shown in Table 3. At the 20% replacement of fly ash in cement paste, the fluidity is obtained as 91 mm. Compared with the FG0 group, the fluidity of samples with 0.2 wt% 3DG is the largest, which is increased by 34.07%. It can be attributed to the following two factors. Firstly, due to the less water demand and containing a lot of smooth spherical particles, fly ash particles take action as a ball between the cement particles to reduce the resistance of cement particles (Wang et al., 2017). As a result, the homogeneity and fluidity of the fly ash cement paste are improved. Secondly, because of the addition of PC with the same mass fraction as 3DG, PC can promote the dispersion of 3DG and enhance the fluidity of the cement-based system. Therefore, fly ash and high-efficiency polycarboxylate superplasticizer can help offset the obstruction of 3DG to the fluidity of cement paste.

3.2.2 Compressive Strength

The effect of 3DG on the compressive strength of fly ash cement-based materials was studied after 28 days of curing. The results are illustrated in Fig. 9. Compared with the OPC sample, the compressive strength of cement paste with a content of 20% fly ash (FG0) has been found to show a slight decrease. Due to the substitution of cement with 20% FA in the FG0 group, the proportion of cement clinker minerals in the system decreases. Therefore, hydrated calcium silicate gel also declines (Shi & Fang, 2004). The compressive strength is reduced accordingly.

Moreover, with the increase of 3DG content, the compressive strength of the paste presents a changing law that first increases and then drops. The compressive strength is improved progressively by increasing the 3DG range from 0.02 to 0.1%. The percentage improvement in compressive strength for FG02, FG05, and FG10 has been observed to be 2.21%, 21.20%, and 31.33% with respect to the FG0 group without 3DG. After that, the compressive strength shows a reduction with the increasing content of 3DG. A similar trend in these results was also found in previous studies (Birenboim et al., 2019). The results demonstrate that the compressive strength can be improved when the content of 3DG does not exceed 0.1%. An appropriate amount of 3DG dispersed in the cement matrix can refine the pore size distribution and adjust the degree of compaction of hydration products. So, the compressive strength of fly ash cement is improved.

3.2.3 Chloride Diffusion

After 7 days of diffusion in sodium chloride solution, the cement samples were axially split and sprayed with

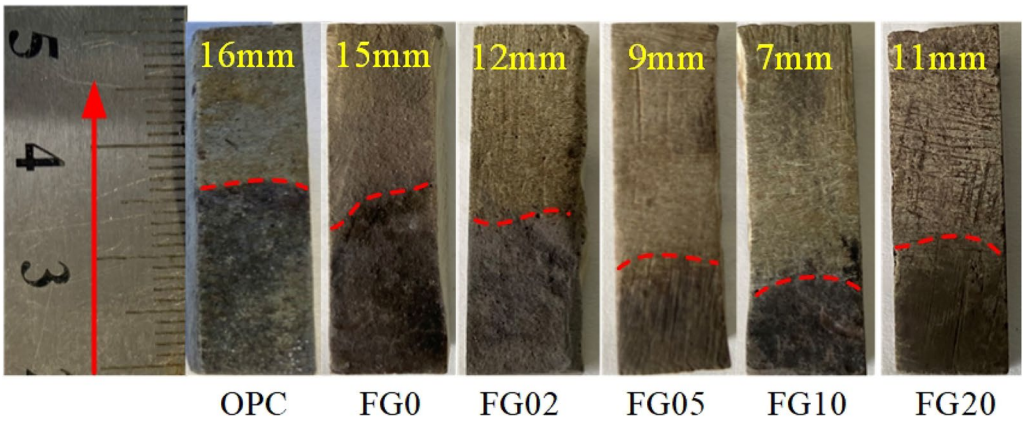

Fig. 10 The diffusion depth of chloride in the splitting surface of fly ash cement paste with different 3DG contents (from bottom to top).

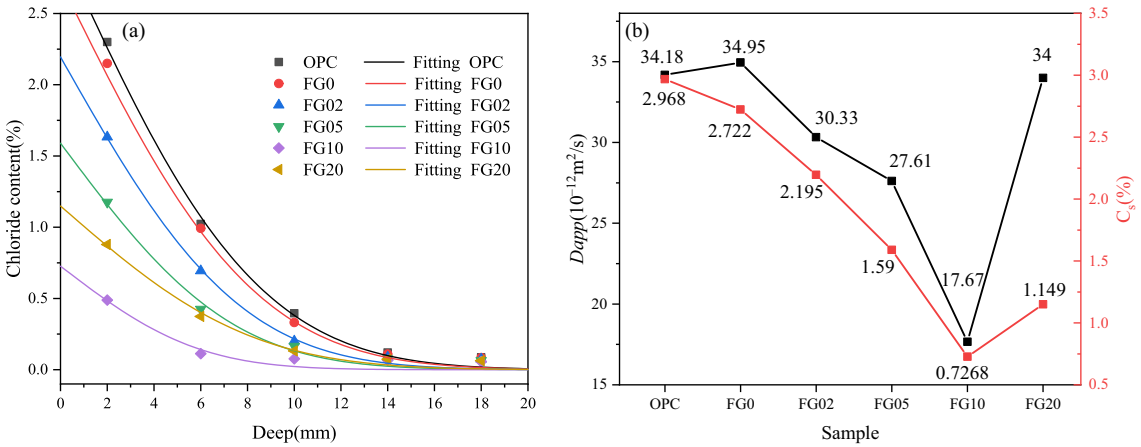

Fig. 11 Chloride diffusion of 3DG-fly ash cement. **a** The chloride concentration and best fit curves; **b** The chloride diffusion coefficient and surface chloride content.

$AgNO_3$. The chloride diffusion depth of fly ash cement paste with different 3DG contents is shown in Fig. 10. The chloride diffusion depth of the OPC group is 16 mm. Compared with the OPC sample, the chloride diffusion depth of the FG0 sample decreases slightly. With the increase of 3DG content, the chloride diffusion depth of fly ash cement drops gradually until 3DG content reaches 0.1%. Comparing to the FG0 samples, the chloride diffusion depth of FG02, FG05, FG10, and FG20 are reduced by 20%, 40%, 53.3%, and 26.67%, respectively.

The diffusion of chloride ions into cement paste can be described by Crank's solution to Fick's second law:

$$C(x,t) = C_0 + (C_S - C_0)\left[1 - \mathrm{erf}\left(\frac{x}{2\sqrt{D_{\mathrm{app}}t}}\right)\right], \quad (1)$$

where $C(x, t)$ is the chloride content at depth x (mm) and time t (s), C_0(%) is the initial chloride ion content in cement, C_S (%) is the chloride content at the surface, the erf is the error function, and $D_{\mathrm{app}}\left(10^{-12}\mathrm{m}^2/\mathrm{s}\right)$ is the chloride diffusion coefficient.

The best-fitted curves of different 3DG contents are displayed in Fig. 11a. It is observed in the figure that the chloride content decreased with the increase of depth. And every sample has the same trend. The chloride diffusion coefficient and surface chloride concentration are shown in Fig. 11b. The chloride diffusion coefficient and chloride content at the cement surface drop gradually until 0.1% and then increase. The chloride diffusion coefficient and chloride content at the cement surface of the FG0 sample are 34.95×10^{-12} m^2/s and 2.722%, respectively. The chloride diffusion coefficient and surface

chloride concentration reduce by 13.22% and 19.36% with the addition of 0.02% 3DG. The minimum chloride diffusion coefficient and surface chloride concentration value are achieved when the 3DG content is 0.1%. Additionally, the chloride diffusion coefficient and surface chloride concentration displayed a maximum reduction of approximately 49.44% and 73.29% compared to the FG0 mix.

In this experiment, the chloride diffusion depth and chloride diffusion coefficient gradually decrease when the content of 3DG is less than 0.1%. It indicates that the appropriate addition of 3DG can effectively improve the barrier performance of fly ash cement composites. This enhancement effect can be attributed to the following three aspects. Firstly, the addition of fly ash and polycarboxylate superplasticizer reduces the viscosity and improves the fluidity of the 3DG-fly ash cement system. It contributes to enhancing the compactness of composite cementitious materials and reducing the generation of pores (Wang et al., 2019a). Secondly, MIP results show that the addition of 3DG significantly enhances the pore structure of fly ash cement-based materials. The pore volume, most probable pore diameter, and the fraction of harmful pores (50–200 nm) are decreased by the addition of 3DG. The decrease in the proportion of macropores restricts the movement of chloride ion molecules into cement-based materials (Du et al., 2016). Finally, 3DG becomes the nucleation point of hydration products with its large surface area, and the shape of hydration products gradually presents a regular and compact appearance. The improvement of hydration product morphology enhances the ability to resist chloride ion diffusion. However, when the dosage of 3DG exceeds 0.1%, the chloride diffusion depth and chloride diffusion coefficient start to increase, which can be attributed to the limitation of the current dispersion technique to disperse high concentration of 3DG uniformly. And the aggregated graphene finally increases the porosity of the system, which reduces the resistance to chloride diffusion.

4 Conclusions

The innovation of this research is that three-dimensional graphene (3DG) with different blending amounts was used in fly ash cement-based materials. In this study, microscopic characterization and macroscopic experiments are carried out. The main conclusions are as follows.

(1) MIP analysis illustrates that the addition of 3DG refines the pore structure distribution in fly ash cement paste. After adding 0.1% 3DG into fly ash cement paste, the most probable pore size reduces from 50.35 nm to 32.39 nm and the fraction of harmful pore decreases from 43.36 to 17.88%. Therefore, the reduction in pore diameter limits the diffusion of chloride.
(2) 3DG can be used as a substrate for crystal formation and deposition because of its huge specific surface area. The addition of 3DG promotes the hydration of cement and then promotes the secondary hydration of fly ash. Moreover, hydration products are filled in cracks and pores, hindering the diffusion of chloride ions. All these effects play a positive role in improving macroscopic properties.
(3) When the content of polycarboxylate superplasticizer remains unchanged, the fluidity of cement paste can be reduced by adding three-dimensional graphene. However, fly ash and polycarboxylate superplasticizer can counteract the adverse effect of graphene on the fluidity of cement paste.
(4) The addition of 3DG improves the compressive strength and chloride diffusion resistance of the fly ash cement system. Compared with the control sample added only fly ash, the hardened fly ash cement paste with 0.1% 3DG has the best performance in compressive strength and chloride diffusion resistance. The 31.33% improvement in compressive strength of fly ash cement composites is achieved, and the chloride ion diffusion depth and the coefficient decrease by 53.3% and 49.44%, respectively.

Acknowledgements
This research is sponsored by the National Natural Science Foundation of China (Grant No. 51768005), Natural Science Foundation of Guangxi (Grant No. 2018GXNSFAA281333), and National Natural Science Foundation of China (Grant No. 52168015).

Authors' contributions
JY contributed to conceptualization, funding acquisition, investigation, project administration, resources, supervision, validation, and writing—review and editing; XX was involved in data curation; JY and XX were involved in formal analysis and methodology;; XX contributed to software and writing—original draft. All the authors read and approved the final manuscript.

Authors' information
Jingwei Ying, associate professor, School of Civil Engineering and Architecture, Guangxi University, Nanning 530004, China.
Xiaoying Xi, Postgraduate Student, School of Civil Engineering and Architecture, Guangxi University, Nanning 530004, China.

Availability of data and materials
The datasets used or analyzed during the current study are available from the corresponding author on reasonable request.

Declarations

Ethics approval and consent to participate
Not applicable.

Consent for publication
All the authors agree that the article will be published after acceptance.

Competing interests
The authors declare that they have no competing interests.

Informed consent
Informed consent was obtained from all individual participants included in this study.

Author details
[1]School of Civil Engineering and Architecture, Guangxi University, Nanning 530004, China. [2]Key Laboratory of Engineering Disaster Prevention and Structural Safety of China Ministry of Education, Guangxi Key Laboratory of Disaster Prevention and Engineering Safety, School of Civil Engineering and Architecture, Guangxi University, Nanning 530004, China.

Received: 1 October 2021 Accepted: 17 December 2021
Published online: 28 January 2022

References

Ariyachandra, E., Peethamparan, S., Patel, S., et al. (2021). Chloride diffusion and binding in concrete containing NO_2 sequestered recycled concrete aggregates (NRCAs). *Construction and Building Materials*. https://doi.org/10.1016/j.conbuildmat.2021.123328

Birenboim, M., Nadiv, R., Alatawna, A., et al. (2019). Reinforcement and workability aspects of graphene-oxide-reinforced cement nanocomposites. *Composites Part B: Engineering, 161*, 68–76.

Du, H., & Dai, P. S. (2015). Enhancement of barrier properties of cement mortar with graphene nanoplatelet. *Cement and Concrete Research, 76*, 10–19.

Du, H., Gao, H. J., & Dai, P. S. (2016). Improvement in concrete resistance against water and chloride ingress by adding graphene nanoplatelet. *Cement and Concrete Research, 83*, 114–123.

Du, H., & Pang, S. D. (2018). Dispersion and stability of graphene nanoplatelet in water and its influence on cement composites. *Construction & Building Materials, 167*, 403–413.

Du, S., Jiang, Y., Zhong, J., et al. (2020). Surface abrasion resistance of high-volume fly ash concrete modified by graphene oxide: Macro-and micro-perspectives. *Construction and Building Materials, 237*, 117686.

Hefni, Y., Abd El Zaher, Y., & Wahab, M. A. (2018). Influence of activation of fly ash on the mechanical properties of concrete. *Construction and Building Materials, 172*, 728–734.

Indukuri, C. S. R., Nerella, R., & Madduru, S. R. C. (2019). Effect of graphene oxide on microstructure and strengthened properties of fly ash and silica fume based cement composites. *Construction and Building Materials, 229*, 116863.

Jiang, W. Q., Shen, X. H., Hong, S., et al. (2019). Binding capacity and diffusivity of concrete subjected to freeze-thaw and chloride attack: A numerical study. *Ocean Engineering*. https://doi.org/10.1016/j.oceaneng.2019.05.075

Kaur, R., & Kothiyal, N. C. (2020). Synergic influence of fly ash and graphene oxide-carbon nanotubes hybrid on mechanical, microstructural and porosity properties of cement mortars. *Journal of Adhesion Science and Technology*. https://doi.org/10.1080/01694243.2020.1860548

Kaur, R., Kothiyal, N. C., & Arora, H. (2020). Studies on combined effect of superplasticizer modified graphene oxide and carbon nanotubes on the physico-mechanical strength and electrical resistivity of fly ash blended cement mortar. *Journal of Building Engineering, 30*, 101304.

Konstantopoulos, G., Koumoulos, E. P., & Charitidis, C. A. (2020). Testing novel portland cement formulations with carbon nanotubes and intrinsic properties revelation: Nanoindentation analysis with machine learning on microstructure identification. *Nanomaterials, 10*, 645.

Lai, K. C., Lee, L. Y., Hiew, B. Y. Z., et al. (2019). Environmental application of three-dimensional graphene materials as adsorbents for dyes and heavy metals: Review on ice-templating method and adsorption mechanisms. *Journal of Environmental Sciences, 79*, 174–199.

Li, G., Huang, B., Pan, Z., et al. (2019). Advances in three-dimensional graphene-based materials: Configurations, preparation and application in secondary metal (Li, Na, K, Mg, Al)-ion batteries. *Energy & Environmental Science, 12*(7), 2030–2053.

Li, G., Yuan, J. B., Zhang, Y. H., et al. (2018). Microstructure and mechanical performance of graphene reinforced cementitious composites. *Composites Part A: Applied Science and Manufacturing, 114*, 188–195.

Li, S. C., Yin, S. P., & Gao, Y. (2020). Analysis of interface properties between TRC and concrete under chloride attack based on fracture energy. *International Journal of Concrete Structures and Materials, 14*(1), 12.

Liu, Q., Wu, W., Xiao, J., et al. (2019). Correlation between damage evolution and resistivity reaction of concrete in-filled with graphene nanoplatelets. *Construction and Building Materials, 208*, 482–491.

Luo, P., Guan, X., Yu, Y., Li, X., & Yan, F. (2019). Hydrothermal synthesis of graphene quantum dots supported on three-dimensional graphene for supercapacitors. *Nanomaterials, 9*, 201.

Lv, S., Liu, J., Sun, T., et al. (2014a). Effect of GO nanosheets on shapes of cement hydration crystals and their formation process. *Construction and Building Materials, 64*, 231–239.

Lv, S., Ma, Y., Qiu, C., et al. (2013). Effect of graphene oxide nanosheets of microstructure and mechanical properties of cement composites. *Construction and Building Materials, 49*, 121–127.

Lv, S., Ting, S., Liu, J., et al. (2014b). Use of graphene oxide nanosheets to regulate the microstructure of hardened cement paste to increase its strength and toughness. *CrystEngComm, 16*(36), 8508–8516.

Mittal, G., Dhand, V., Rhee, K. Y., et al. (2015). Investigation of seawater effects on the mechanical properties of untreated and treated MMT-based glass fiber/vinylester composites. *Ocean Engineering, 108*, 393–401.

Morga, M., & Marano, G. C. (2015). Chloride penetration in circular concrete columns. *International Journal of Concrete Structures and Materials, 9*(2), 173–183.

Muthu, M., Yadav, S., & Schneider, J. J. (2021). Investigation of the changes in properties and microstructure of graphene oxide-modified cement pastes due to hydrochloric acid attack. *Journal of Sustainable Cement-Based Materials, 2021*, 17.

Nguyen, P. T., Bastidas-Arteaga, E., Amiri, O., & El Soueidy, C. P. (2017). An efficient chloride ingress model for long-term lifetime assessment of reinforced concrete structures under realistic climate and exposure conditions. *International Journal of Concrete Structures and Materials, 11*(2), 199–213.

Park, S., & Choi, Y. (2012). Influence of curing-form material on the chloride penetration of off-shore concrete. *International Journal of Concrete Structures and Materials, 6*(4), 251–256.

Sharma, S., Susan, D., Kothiyal, N. C., & Kaur, R. (2018). Graphene oxide prepared from mechanically milled graphite: Effect on strength of novel fly-ash based cementitious matrix. *Construction and Building Materials, 177*, 10–22.

Shen, D. S., & Zhang, J. M. (1981). A study of the effects of fly ash. *Journal of the Chinese Ceramic Society, 01*, 57–63.

Shen, P. K., Li, Y. Y., Tian, Z. Q., et al. (2016). A preparation method of graphene powder with three-dimensional multistage pore structure, CN105923623A [P/OL]. 2016-09-07.

Shi, H. S., & Fang, Z. F. (2004). Influence of fly ash on early hydration and pore structure of cement pastes. *Journal of the Chinese Ceramic Society, 01*, 95–98.

Tragazikis, I. K, Dassios, K. G., Dalla, P. T., et al. (2019). Acoustic emission investigation of the effect of graphene on the fracture behavior of cement mortars. *Engineering Fracture Mechanics, 210*, 444–451.

Wang, M., Wang, R., Yao, H., et al. (2016). Study on the three dimensional mechanism of graphene oxide nanosheets modified cement. *Construction and Building Materials, 126*, 730–739.

Wang, Q., Cui, X., Wang, J., Li, S., Lv, C., & Dong, Y. (2017). Effect of fly ash on rheological properties of graphene oxide cement paste. *Construction and Building Materials, 138*, 35–44.

Wang, Q., Li, S., Pan, S., Cui, X., Corr, D. J., & Shah, S. P. (2019a). Effect of graphene oxide on the hydration and microstructure of fly ash-cement system. *Construction and Building Materials, 198*, 106–119.

Wang, Y., Guo, L., Qi, P., Liu, X., & Wei, G. (2019b). Synthesis of three-dimensional graphene-based hybrid materials for water purification: A review. *Nanomaterials, 9*, 1123.

Wu, W., Wang, R., Zhu, C., et al. (2018). The effect of fly ash and silica fume on mechanical properties and durability of coral aggregate concrete. *Construction and Building Materials, 185*, 69–78.

Wu, Z. W. (1979). Discussion on the recent development direction of concrete science and technology. *Journal of the Chinese Ceramic Society, 3*, 82–90.

Yamato, K., Sasaki, A., Ito, T., & Yoshitake, I. (2020). Resistance properties to chloride ingress of standard-cured concrete made with an admixture

incorporating rich SiO_2 and Al_2O_3. *International Journal of Concrete Structures and Materials, 14*(1), 11.
Yu, Z., Ma, J., Ye, G., et al. (2017). Effect of fly ash on the pore structure of cement paste under a curing period of 3 years. *Construction and Building Materials, 144*, 493–501.
Zhang, A., Ge, Y., Yang, W., et al. (2019). Comparative study on the effects of nano-SiO_2, nano-Fe_2O_3 and nano-NiO on hydration and microscopic properties of white cement. *Construction and Building Materials, 228*, 116767.
Zhang, S., Qiao, W. G., Chen, P. C., et al. (2019). Rheological and mechanical properties of microfine-cement-based grouts mixed with microfine fly ash, colloidal nano silica and superplasticizer. *Construction and Building Materials, 212*, 10–18.
Zhao, L., Hou, D., Wang, P., et al. (2020). Experimental and molecular dynamics studies on the durability of sustainable cement-based composites: Reinforced by graphene. *Construction and Building Materials, 257*, 119566.
Zhao, Y., Qiu, J., Zhengyu, M. A., et al. (2020). Effect of superfine blast furnace slags on the binary cement containing high-volume fly ash. *Powder Technology*. https://doi.org/10.1016/j.powtec.2020.07.094

Publisher's Note